

# Mars Climate Sounder: An investigation of thermal and water vapor structure, dust and condensate distributions in the atmosphere, and energy balance of the polar regions

D. J. McCleese,<sup>1</sup> J. T. Schofield,<sup>1</sup> F. W. Taylor,<sup>2</sup> S. B. Calcutt,<sup>2</sup> M. C. Foote,<sup>1</sup> D. M. Kass,<sup>1</sup> C. B. Leovy,<sup>3</sup> D. A. Paige,<sup>4</sup> P. L. Read,<sup>2</sup> and R. W. Zurek<sup>1</sup>

Received 7 July 2006; revised 21 September 2006; accepted 8 December 2006; published 31 May 2007.

[1] Against a backdrop of intensive exploration of the Martian surface environment, intended to lead to human exploration, some aspects of the modern climate and the meteorology of Mars remain relatively unexplored. In particular, there is a need for detailed measurements of the vertical profiles of atmospheric temperature, water vapor, dust, and condensates to understand the intricately related processes upon which the surface conditions, and those encountered during descent by landers, depend. The most important of these missing data are accurate and extensive temperature measurements with high vertical resolution. The Mars Climate Sounder experiment on the 2005 Mars Reconnaissance Orbiter, described here, is the latest attempt to characterize the Martian atmosphere with the sort of coverage and precision achieved by terrestrial weather satellites. If successful, it is expected to lead to corresponding improvements in our understanding of meteorological phenomena and to enable improved general circulation models of the Martian atmosphere for climate studies on a range of timescales.

**Citation:** McCleese, D. J., J. T. Schofield, F. W. Taylor, S. B. Calcutt, M. C. Foote, D. M. Kass, C. B. Leovy, D. A. Paige, P. L. Read, and R. W. Zurek (2007), Mars Climate Sounder: An investigation of thermal and water vapor structure, dust and condensate distributions in the atmosphere, and energy balance of the polar regions, *J. Geophys. Res.*, **112**, E05S06, doi:10.1029/2006JE002790.

## 1. Introduction

[2] The Mars Climate Sounder (MCS) represents NASA's third attempt to observe Martian weather and monitor the planet's climate using modern infrared remote sensing techniques, including limb sounding. The campaign began in 1986 with the Pressure Modulator Infrared Radiometer (PMIRR) [McCleese *et al.*, 1986, 1992] on the Mars Observer mission, which was lost in 1993 during the final pressurization of the spacecraft propulsion system only a few days prior to Mars orbit insertion (MOI). NASA re-selected that scientific investigation, including an enlarged science team and using the same PMIRR instrument design, for another mission, the Mars Climate Orbiter (MCO). Launched in 1998, the MCO spacecraft entered the Martian atmosphere during MOI and was destroyed. NASA selected our team once more to build the new MCS instrument now onboard the Mars Reconnaissance Orbiter (MRO). MCS is not a copy of the PMIRR instrument launched in 1992, as the 1998 PMIRR II was, but is a smaller, lighter instrument

with the same scientific objectives as those of the previous two investigations.

[3] Significant strides have been made in understanding the meteorology and present climate of Mars [Leovy, 2001]. The Viking surface meteorology packages [Tillman, 1988; Hess *et al.*, 1977] provided nearly continuous records of atmospheric pressure for 3.5 years at VL 1 (23°N) and 1.5 years at VL2 (48°N). This unique planetary meteorology data set, together with earlier measurements of the vertical structure of temperature from Mariner 9 [Hanel *et al.*, 1972], provided a touchstone for modelers of Martian atmospheric dynamics and transport for more than 20 years. Another major step forward came in 1997 when the Mars Global Surveyor's Thermal Emission Spectrometer (TES) [Christensen *et al.*, 2001], the Mars Orbiter Camera (MOC) [Malin and Edgett, 2001], and Radio Science (RS) [Tyler *et al.*, 2001] began to return atmospheric thermal structure data, as well as observations of the distributions of cloud and dust. Formisano *et al.* [2005] are now accumulating a high spectral resolution thermal data set from the Mars Express orbiter. Additional measurements by landed probes during their descent and on the surface have been obtained by Viking, Pathfinder, and MER entry probes [Seiff and Kirk, 1977; Magalhães *et al.*, 1999; Schofield *et al.*, 1997; Withers and Smith, 2006]. Taken together, data from the MGS payload provide a global picture of the Martian atmosphere (climatology of four full Mars years). The nearly continuous global coverage and quality of the TES data set are such that retrieved temperatures are now being

<sup>1</sup>Jet Propulsion Laboratory, California Institute of Technology, Pasadena, California, USA.

<sup>2</sup>Department of Physics, University of Oxford, Oxford, UK.

<sup>3</sup>Department of Atmospheric Sciences, University of Washington, Seattle, Washington, USA.

<sup>4</sup>Department of Earth and Space Sciences, University of California, Los Angeles, Los Angeles, California, USA.

**Table 1.** MCS Observation Modes and Science Objectives

Observation Mode	Measurement Objective	Science Objective	High-Level Science Goal
In Track Limb Staring	Vertical profiles of temperature, pressure, aerosols, and water vapor	Global monitoring of atmospheric properties	Atmospheric circulation, interannual climate variations, annual water, and dust cycles
Nadir Sounding	Surface infrared radiance and broadband solar reflectance	Characterization of surface and sub-surface thermal state and thermal properties	Climate, distribution, and state of surface and subsurface water
Polar Buckshot Scanning	Net polar radiative balance	Annual carbon dioxide frost budget	Interannual and secular climate variations, and global change

assimilated into numerical schemes that include the physics governing the state of the atmosphere. Potentially, assimilation of sounder and other data types will permit the study of spatial and temporal domains, as well as components of the atmosphere not directly observed [see *Lewis and Read, 1995; Lewis et al., 1997*]. Experiments with assimilating remote sensing data from TES represent a first application to planetary research of a well-honed technique for Earth meteorology and weather forecasting.

[4] The global and seasonal distributions of water vapor in the Martian atmosphere have received special attention due, in large part, to the role water plays in sustaining life. Measurements of daytime column water abundance by *Farmer et al. [1979]* and *Jakosky and Farmer [1982]* using the Mars Atmospheric Water Detector (MAWD) on the Viking orbiters revealed the strong seasonal exchange of water between the atmosphere and polar ice. The TES instrument contributes again by extending column water vapor measurements over multiple annual cycles [*Smith, 2002*]. Whether sources and sinks of atmospheric water vapor exist away from the poles remains unexplored. This question took on more significance recently when subsurface hydrogen (indicative of near surface ice) was mapped away from the residual caps by the Gamma Ray Spectrometer on MGS [*Boynton et al., 2002; Mitrofanov et al., 2002*]. If this reservoir of ice, or others at mid and low latitudes, is currently exchanging water with the atmosphere, mechanisms for emplacing and recharging the ice become important for their longer-term climatological implications.

[5] Although observations of the atmosphere from orbit, and from the surface, span nearly 30 years, the data record is not continuous. The 20-year hiatus in missions to Mars following Viking was an unfortunate interruption. However, the continuity of observations is excellent beginning with MGS. Since 1997, year-to-year variability of the atmosphere has been reported by MGS investigator teams and by others looking for interannual variability [*Cantor et al., 2002*]. For the nearly 100 years prior to MGS, ground-based telescopic observations identified significant atmospheric variability on various time-scales, most of which is now recognized to be related to varying amounts of dust in the atmosphere. Most dramatic and easily detected from Earth is the quasiperiodic variability in the visibility of surface features due to large-scale dust storms [*Zurek and Martin, 1993*]. Recently, *Cantor et al. [2002]* reported details of the visible morphology of individual dust storms. MOC imagery shows that these storms appear at almost all spatial scales from 1 km to global in extent, and the occurrence of local dust storms is more frequent than previously thought. *Malin et al. [2001]* suggest that variability in surface features may also be

indicative of climate change on annual and much longer timescales. Particularly interesting are two pieces of evidence possibly related to climate change revealed in surface ice; the polar layered terrain possibly linked with period changes in the obliquity of Mars [*Ward, 1973; Laskar and Robutel, 1993*], and discovery of year-to-year variation in the appearance of features in polar CO<sub>2</sub> ice [*Cantor et al., 2002*].

[6] A major feature of the modern Martian climate is the cycling of a large fraction of the mass of the atmosphere through the seasonal polar caps. Very large exchanges of radiative, sensible and latent heat must be involved, although the details of the processes at work are obscure. An objective of MCS is to understand the temporally and spatially resolved energy balance of the polar regions through measurements of the ingoing solar and outgoing thermal radiative fluxes at the top of the atmosphere, and hence to constrain models of the local and global CO<sub>2</sub> cycle.

### 1.1. Mars Climate Sounder Investigation

[7] MCS is an investigation designed to acquire the high vertical resolution, horizontally contiguous measurements needed to take the next major step forward in understanding the Martian atmosphere. MCS will measure thermal emission from the limb of the atmosphere in nine spectral bands to obtain profiles with a vertical resolution of 5 km (approximately one half the atmospheric scale-height on Mars). The MCS investigation will invert accurately calibrated measurements of radiance in profiles extending from the surface to an altitude of 80 km to obtain vertical profiles of atmospheric temperature, water vapor abundance, and dust and condensate opacities. MCS will also acquire nadir and off-nadir observations that provide additional constraints on atmospheric profiles, and measurements of infrared thermal emission and broadband solar reflectance of the surface. In the polar regions, more frequent nadir and off-nadir measurements will be used to characterize the radiation balance at the top of the atmosphere, which provides constraints on the rates of condensation and sublimation of CO<sub>2</sub> on the surface and in the atmosphere.

[8] The MCS science team intends to utilize these measurement capabilities to address the MRO mission's objectives for the atmosphere and climate, specifically to "advance our understanding of Mars' current climate, the processes that have formed and modified the surface of the planet, and the extent to which water has played a role in surface processes."

[9] The MCS investigation will "assess Mars' seasonal and time-of-day variations in water, dust, and carbon dioxide in the atmosphere; and characterize Mars' global atmospheric structure and surface changes." Table 1 is a

high-level description of the instrument observation modes and the objectives that they address.

## 1.2. Climatology for Mars

[10] The MCS investigation approach to characterizing the present climate of Mars is to collect an extended record of the daily temperature, dust, water vapor, and condensates structure. When appended to the record begun in 1997 by MGS and complemented by Mars Odyssey, and by Mars Express, the climate record will extend without interruption for six Martian years. Nothing in the design of the MRO spacecraft, in propellant reserves for orbit maintenance, or in the MCS instrument precludes two additional Martian years of continuous monitoring being added to the record.

[11] In addition to extending the climatology, MCS brings important improvements and new quantities to the record. MCS observes the limb of the atmosphere repetitively, affording better vertical resolution than has been available thus far; the observations will have an extended vertical range; and the observations will be nearly continuous along the spacecraft track, orbit after orbit, and day after day. MCS measurements of vertical profiles of water vapor and dust will be the first in the record. Detailed discussions of the MCS observation scheme and the impacts of off-nadir pointing by the spacecraft are presented in section 4.

[12] The MCS instrument is described in section 3 together with results from ground testing and characterization measurements performed prior to launch. Section 5 includes early demonstration observations of Mars from MCS taken just days after MRO orbit insertion. In section 6, we describe how MCS measurements will be used by the MCS science team in their research.

## 2. Investigation Description

[13] In 1999, following the failure of the MCO spacecraft, a major redesign of the instrument was undertaken by the science team. The result is a much-reduced instrument mass, a smaller footprint on the payload deck, fewer mechanisms, and lower power requirements. PMIRR was a 44-kg instrument consuming 40 W. MCS weighs 9 kg and consumes 11 W of continuous power.

[14] The elements of the PMIRR instrument that most drove its overall size and mass were the HgCdTe detector focal plane, the pressure modulator units, and the scan mirror assembly. The focal plane operated at a temperature of  $\leq 90$  K requiring a large and massive radiative cooler. The cooler required a clear view of space, which presented challenges for the configuration of the spacecraft payload deck. Two pressure modulator units [Taylor *et al.*, 2006] were mounted on the PMIRR optical bench: one containing CO<sub>2</sub> for measurements of atmospheric temperature, and the other containing H<sub>2</sub>O for profiling water vapor abundance in the Martian atmosphere. The availability of new high performance, linear array thermopile detectors with focal plane signal processing [Foote *et al.*, 2003] was the key that made possible a much-simplified design for MCS without compromising performance.

### 2.1. Thermopile Detector and Filter Technologies Enable a Compact MCS

[15] With a linear array of detectors, MCS obtains vertical profiles by staring at the limb, whereas PMIRR utilized

frequent stepping of the field of view (FOV) of individual detectors to profile the atmosphere. Limb staring is advantageous because it lengthens measurement dwell times for each element in the vertical profile, thus increasing signal-to-noise performance. Although the performance of room temperature thermopile detectors is not equal to that of the cooled HgCdTe detectors used in PMIRR, limb staring and a higher optical throughput give MCS the desired measurement capability to accomplish its objectives.

[16] Elimination of the radiative cooler, the substitution of filter channels for pressure modulator units, the reduction in signal processing electronics mass and power, and a new compact optical design make MCS small enough for the whole instrument to be articulated. A consequence of the new optical design was the need to develop small, high aspect ratio ( $0.94 \times 9.0$  mm) spectral band-pass filters. High aspect ratio, long wavelength 30  $\mu$ m to 45  $\mu$ m passband conductive mesh filters were developed for MCS by the Cardiff University [Irwin *et al.*, 1993]. Multilayer interference filters for 12  $\mu$ m to 17  $\mu$ m wavelengths were developed by the University of Reading [Hawkins and Hunneman, 1994]. While both filter types are in common use in a variety of instrument types, the MCS configuration is new.

### 2.2. Measurement Approach

[17] Remote sensing of atmospheric state and the abundances of atmospheric constituents from orbiting platforms has a decades long history of application to Earth and planetary atmospheres [see, for example, Houghton and Taylor, 1973]. Numerous techniques have been employed, most frequently operating at infrared and microwave wavelengths. For Mars, infrared Michelson interferometers have been the technique of choice to date. The Mariner 9, infrared interferometer spectrometer (IRIS) [Hanel *et al.*, 1972] provided the first detailed information on the thermal structure and dust opacity of the atmosphere. The Thermal Emission Spectrometer (TES) onboard the MGS orbiter accumulated almost three Mars years of observations of atmospheric temperature, dust, and water vapor column abundance [Smith *et al.*, 2001; Smith, 2002]. Because of its broad spectral coverage, 200 to 1650  $\text{cm}^{-1}$ , spectral resolution, 5 to 10  $\text{cm}^{-1}$ , and nadir to limb scanning, TES has been enormously successful in a variety of investigations of Mars, e.g., mineralogy, thermal inertia, atmospheric structure. Filter radiometers, such as MCS, trade spectral resolution for higher signal levels, enabling high vertical resolution sufficient to resolve one half the Martian atmospheric scale-height. An additional trade is the nearly continuous observation of the atmosphere by MCS: unlike other instruments that focus on surface science, the prime objective of MCS is the atmosphere. Finally, MCS is designed with radiometric calibration foremost among its requirements, not a strength of many other infrared sensing techniques.

[18] MCS employs a nearly continuous limb viewing strategy in order to achieve greatly increased sensitivity to minor and trace constituents, the atmospheric limb path length being approximately 50 times that of a nadir view on Mars. The vertical resolution is also improved compared with the vertical resolution achievable by nadir viewing instruments. Martian targets of interest to the MCS investigation are typically low radiance, such as the cold low-emittance atmosphere and low temperature surfaces ( $<150$  K



**Table 2.** MCS Spectral Channel Band Passes and Measurement Functions<sup>a</sup>

Telescope/ Channel Number	Band Pass, cm <sup>-1</sup>	Band Center, μm	Measurement Function
A1	595–615	16.5	temperature 20 to 40 km
A2	615–645	15.9	temperature 40 to 80 km and pressure
A3	635–665	15.4	temperature 40 to 80 km and pressure
A4	820–870	11.8	dust and condensate (D&C) extinction 0 to 80 km
A5	400–500	22.2	temperature 0 to 20 km, D&C extinction 0–80 km
A6	3300–33000	1.65	polar radiative balance
B1	290–340	31.7	temperature 0 to 20km and D&C extinction 0 to 80 km
B2	220–260	41.7	water vapor 0 to 40 km and D&C extinction 0 to 80 km
B3	230–245	42.1	water vapor 0 to 40 km and D&C extinction 0 to 80 km

<sup>a</sup>D is dust; C is condensates of H<sub>2</sub>O and CO<sub>2</sub>.

in the polar night). This is another factor that led to the selection of a radiometer design that favors large energy grasp over spectral resolution. MCS measurements are made in nine spectral intervals with 20 cm<sup>-1</sup> and broader spectral passbands in the range 0.3–45 μm; see Table 2.

[19] When compared with nadir sounding, limb sounding sacrifices horizontal resolution for high vertical resolution. Horizontal resolution is typically no better than 200 km along a limb path at Mars. Long atmospheric paths can also be detrimental to atmospheric sounding in instances where highly absorbing or scattering constituents are present. Such is the case when large amounts of dust are present in the Martian atmosphere. For these reasons, MCS intersperses frequent views of nadir with its limb observations. The instantaneous FOV is 5 km vertical × 8.6 km horizontal at the limb and 1 km × 1.7 km at the surface from the anticipated mean MRO orbital altitude of 288 km.

### 3. Instrument Description

[20] The MCS flight instrument is shown in Figure 1 with all of its major elements labeled. The instrument consists of

an optical bench assembly (OBA), containing the optics bench, telescopes, and analog and digital electronics boards, suspended from a yoke via the elevation actuator. The yoke supports the instrument, accommodates instrument calibration targets and power conditioning and drive electronics, and provides the mechanical and electrical interface with the spacecraft via a twist-capsule mounted on the azimuth actuator. A similar twist capsule, mounted on the elevation actuator assembly, conveys power and signals between the yoke and OBA electronics. Table 3 summarizes the primary physical and operational parameters of the instrument.

#### 3.1. Instrument Overview

[21] The MCS telescopes and optical bench are shown in cross section in Figure 2. The entire MCS optical bench is articulated in two axes in order that the limb as well as the nadir can be observed. The range of articulation is 270° in both azimuth and elevation axes providing views of the full hemisphere beneath the nadir-pointed payload platform.

[22] Each telescope consists of mirrors and a focal plane assembly supported by a metering structure, which is suspended within the instrument optical bench. The two



**Figure 1.** The MCS flight instrument photographed during calibration at JPL. Major elements of the instrument are identified.

**Table 3.** MCS Instrument Specifications

Parameter	Property/Performance
Instrument type	Filter radiometer
Spectral range and channels	0.3 to 45.0 $\mu\text{m}$ in nine spectral channels
Telescopes	two identical, 4 cm aperture, f/1.7 telescopes
Detectors	nine arrays near 290 K
Fields of view	Detector IFOV: 3.6 $\times$ 6.2 mrad 5.0 $\times$ 8.6 km (at limb) Instrument IFOV: 75 $\times$ 75 mrad 105 $\times$ 105 km (at limb)
Instrument articulation	two-axis azimuth/elevation range/resolution: Azimuth: 270/0.1 $^\circ$ Elevation: 270/0.1 $^\circ$
Operation modes	Single Operating Mode, 2.048s signal integration period
Observation strategy	Limb Staring; limb, nadir and off-nadir scanning in-track, cross-track, and off-track viewing

identical MCS telescopes are differentiated primarily by their focal planes. Telescope A has a focal plane with six spectral channels, labeled A1 through A6 in Table 2. These visible and mid-IR channels are defined spectrally by optical interference filters mounted over six, 21-element linear thermopile detector arrays. The telescope B focal plane has three far-infrared spectral channels, defined spectrally by conductive mesh filters mounted over three detector arrays. Figure 3 shows a schematic of the nominal FOV response of the MCS detectors, superimposed on the limb of Mars, with the filters and spectral channel assignments also indicated. The telescope optical design is discussed in more detail in section 3.2.

[23] Each MCS focal plane assembly consists of a detector chip, focal plane signal processing chips, and a band-pass filter assembly, all mounted on a focal plane block. An overview of the focal plane assembly is given in section 3.3, followed by more detailed descriptions of the band-pass filters, and the focal plane detectors and signal processing (section 3.4). MCS articulation is described in more detail in section 3.5, and a brief overview of the instrument electronics, software, and digital signal processing is given in section 3.6. Finally the provisions in the MCS design for the in-flight radiometric calibration of the infrared and visible spectral channels are discussed in section 3.7.

### 3.2. Instrument Optical Design/Telescopes

[24] An optical schematic of one of the two telescopes is presented in Figure 4. The telescopes are of identical design. Both are off-axis, all-reflective, telecentric with 4 cm apertures, FOVs of 4.3 $^\circ$ , and comprising three mirrors. The telescopes are mounted with parallel optical axes; rotated 180 $^\circ$  relative to each other about their prime axes (Figure 2). The instrument aperture is defined by the perimeter of the secondary mirror and the tertiary mirror focuses an f/1.7 beam through band-pass filters and baffles on to the focal plane detectors. The baffles, mounted close to the back surfaces of the filters, act as light pipes for the detectors and define the FOV response of the individual detector elements. Limb-sounding atmospheric measurements with the resolution required by MCS place fairly modest requirements on image quality but are strongly influenced by the far wings of the FOV response in the vertical direction. Focal plane baffles reduce FOV response

wings produced by scattering within the filters and by thermal radiation re-emitted from the detectors. Also, the secondary mirror is apodized at the edges, using deposited gold black, to reduce FOV wings caused by diffraction at the longer wavelengths.

[25] The telescope mirrors are diamond turned from nickel-plated aluminum and post-polished to reduce scattering at visible wavelengths. The reflective surface is a silicon dioxide-protected aluminum coating, chosen for its reflectivity at both visible and infrared wavelengths and its robustness. The aluminum metering structure supports the mirrors and its internal surfaces form baffles that shield the space between the tertiary mirror and the focal plane (Figure 4). An external baffle, mounted on the optical bench, prevents stray light reaching the focal plane after only one reflection (Figure 4). All the exposed internal surfaces of the metering structure and external baffle are treated with Martin Black to reduce scattering. Alignment tolerances for the MCS telescope permit a “snap together” design, although provisions are made for shimming the primary mirror and focal plane. In practice, only the focal plane is adjusted to achieve best focus.

[26] Because MCS is an unchopped radiometer, considerable care is taken to minimize thermal drifts in the

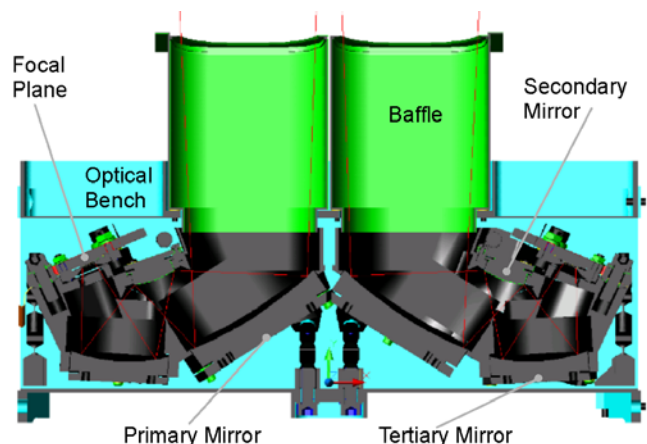


**Figure 2.** Mechanical cross section of MCS telescopes and optical bench.

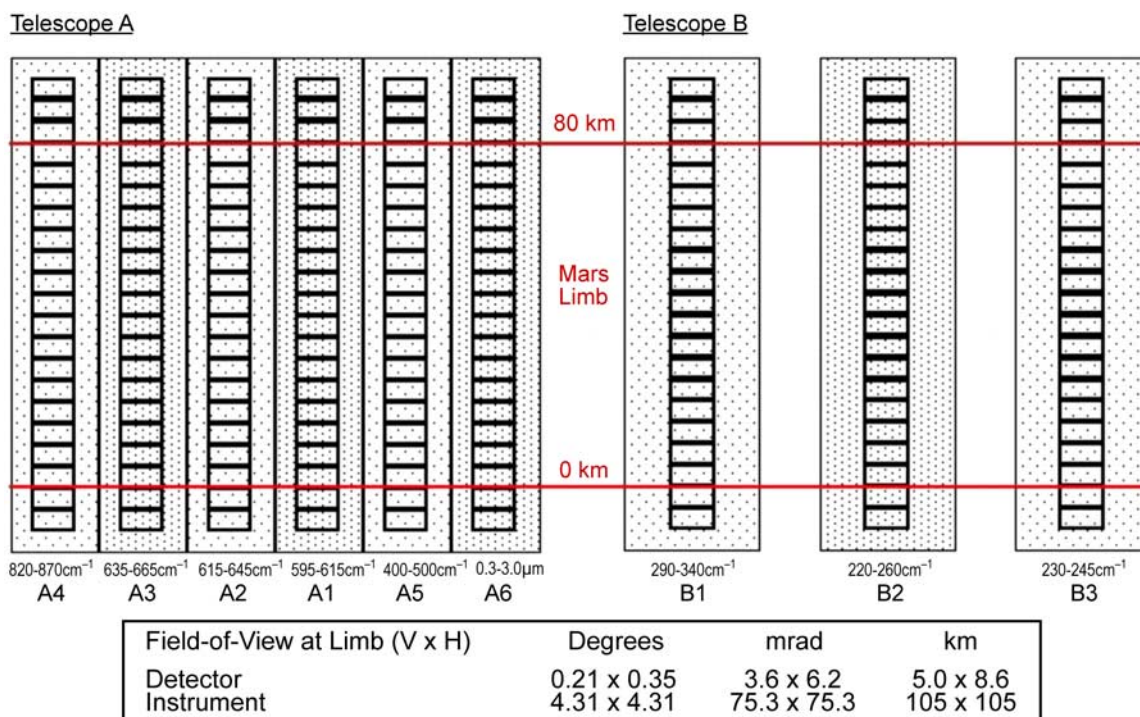


**Figure 3.** MCS fields of view projected at the limb of Mars. The telescope A and B FOV responses are aligned to be superimposed within one-half FOV in the horizontal dimension and one-tenth FOV in the vertical (shown separated in figure for clarity).

telescope and focal plane assembly. The primary source of variable radiant energy that will tend to destabilize the instrument temperature is exposure, once per orbit, to the large day-night contrast in solar illumination and Martian surface temperature. High thermal stability is achieved in MCS by maximizing the thermal mass of the telescope, maximizing the thermal conductivity between its component parts, and conductively isolating the telescopes from the surrounding optical bench, which sees most of the variable environmental heat load from the instrument thermal blankets and external baffles. The MCS telescopes are each mounted at three points to the optical bench via struts with flexures. Conductive isolation between the struts and optical bench is provided by fiberglass (G10) washers. Temperature control is applied to the optical bench, which acts as a stable radiative “oven” for the telescopes and focal planes. The stable thermal environment, all aluminum mirrors and metering structure, and flexured interfaces with the optical bench and focal plane assembly also minimize thermal distortion in telescope alignment.

### 3.3. Focal Plane Filters

[27] The spectral passbands of MCS are defined using individual spectral filters mounted in metal frames in front of each of the 9 detector arrays (Figure 5). For telescope A, the five mid-infrared filters in the focal plane cover the 11.8- to 22.2- $\mu\text{m}$  wavelength range (channels A1 through A5). These are multilayer interference filters manufactured by the University of Reading, UK. Germanium was the substrate material of choice for the five mid-infrared filters (A1 through A5) because of its robust mechanical properties and high optical transmission over the full spectral range. The Germanium absorption band near 20  $\mu\text{m}$  was not a

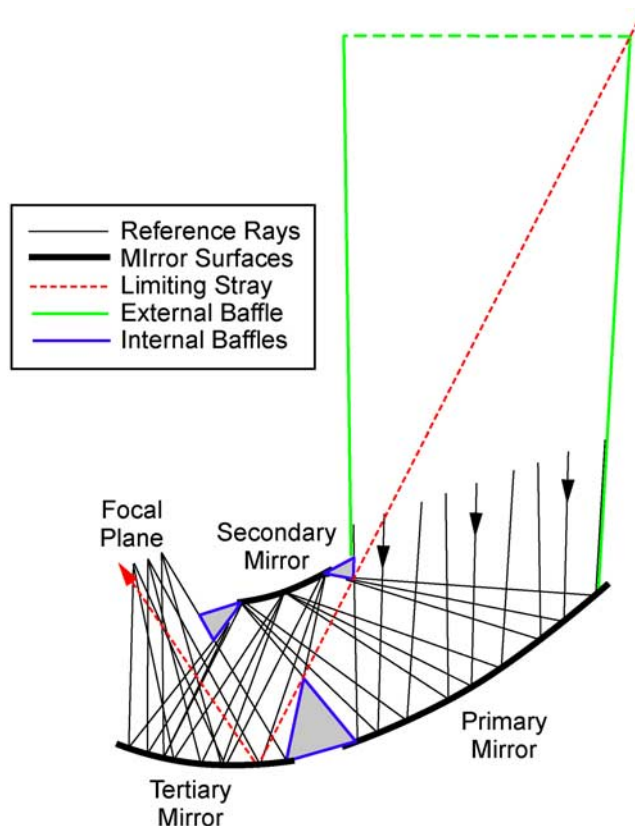


**Figure 4.** MCS telescope optical schematic and baffle approach.



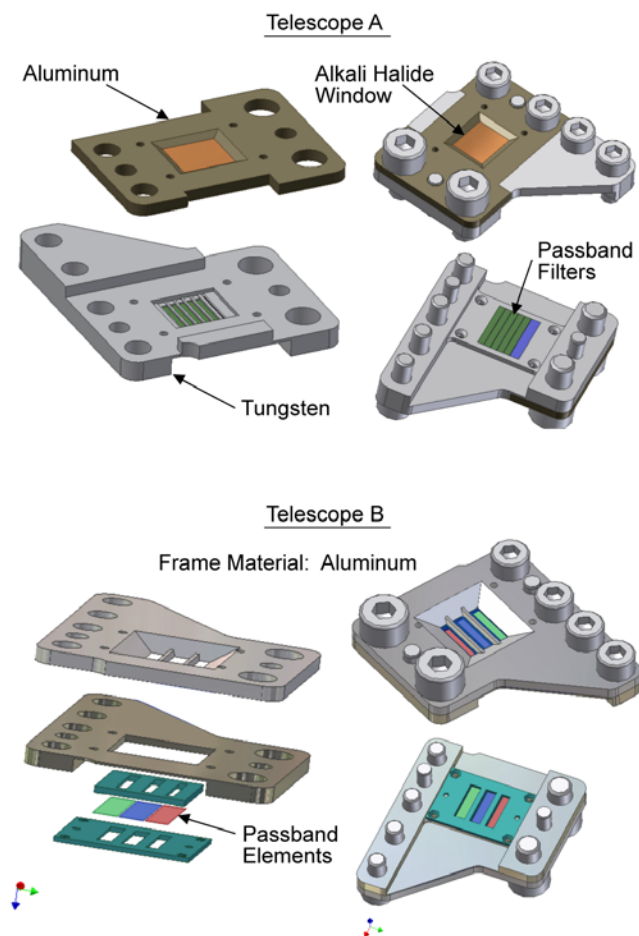


**Figure 5.** MCS filter assemblies.

major concern because the substrates are very thin. The multilayer filters are of conventional design but they are unusually small and five filters must fit directly over the MCS focal plane. Small filters are cut from a larger substrate. Good yield was achieved with this approach with little chipping or other damage to the substrates or coatings. The broadband 0.3 to 3  $\mu\text{m}$  filter, A6, is made of UV22 glass, chosen for its blocking from 3 to 5  $\mu\text{m}$ .

[28] The three far infrared filters in focal plane B consist of stacks of mesh filters developed by Cardiff University. The same group successfully produced air spaced mesh filters for the PMIRR instruments. Cardiff produced a “hot pressed” version of their filters consisting of copper meshes on polypropylene substrates, which can be cut to fit the smaller MCS filter frames.

[29] Thermal stability of all the spectral filters is critical. The MCS thermopile arrays respond to radiation at all wavelengths where their surfaces absorb, i.e., where gold black has low reflectivity. Small excursions in the temperature of the filters will produce measurable signals, because the filters themselves are sources of blackbody radiation at all wavelengths away from their narrow spectral windows. Temperature changes in the filters due to the changing scene, e.g., Mars and the limb of the atmosphere, are potentially large enough to cause a measurable, but spurious, effect. Note that the filters fill nearly the whole  $2\pi$  FOV of the detector. A change in the temperature of 5 mK

produces a spurious signal equivalent to a 1% true signal change in channel A3. Consequently, it is essential that the filters be mounted in good thermal contact with a large thermal mass.

[30] The filter assemblies throughout the instrument incorporate aluminum alloy baffles located between the detectors and the filters to reduce the transmission of off-axis rays produced from reflections within the assemblies and by reflection and emission from the detector surfaces. These baffles, produced using EDM (Electrical Discharge Machining), have the same external dimensions as the detector arrays with individual cell walls surrounding the each of the individual detectors. The baffles have an anodized coating with low large angle reflectivity that preferentially reduces off-axis reflections.

### 3.4. Detectors and Signal Processing

[31] The MCS focal plane assembly A (FPA-A) comprises six arrays with two front-end signal read-out chips and FPA-B three arrays and one chip. The detector arrays are micro-machined thermopile arrays using Bi-Sb-Te and Bi-Te thermoelectric materials. The fabrication process used is similar to that described by Foote *et al.* [1998]. Figure 6 shows a single MCS thermopile detector pixel; the gold black light-absorbing coating has yet to be applied to the detector surface in this image. Each pixel consists of a silicon-nitride membrane with twelve Bi-Sb-Te/Bi-Te thermocouples connected in series. These thermocouples measure the temperature difference between the thermally isolated absorber and the substrate. The thick dark lines in Figure 6 indicate slits through the membrane that separate each pixel from neighboring pixels and define the pixel. The detectors are coated with gold black, providing high absorptivity and nearly flat spectral response from 0.3 to 45  $\mu\text{m}$ . During deposition, the gold black forms bridges across the membrane slits, thermally shorting detectors to each other and to the substrate. These unwanted gold black bridges are eliminated by laser ablation from the detector backside with 248 nm excimer laser radiation. The detector membrane acts a mask during this ablation process to confine the laser energy to the gold black bridges. It is

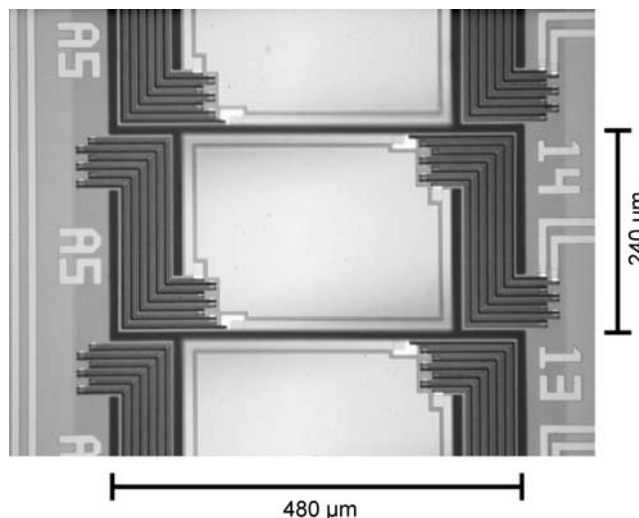


**Figure 6.** Unblackened MCS thermopile detectors.

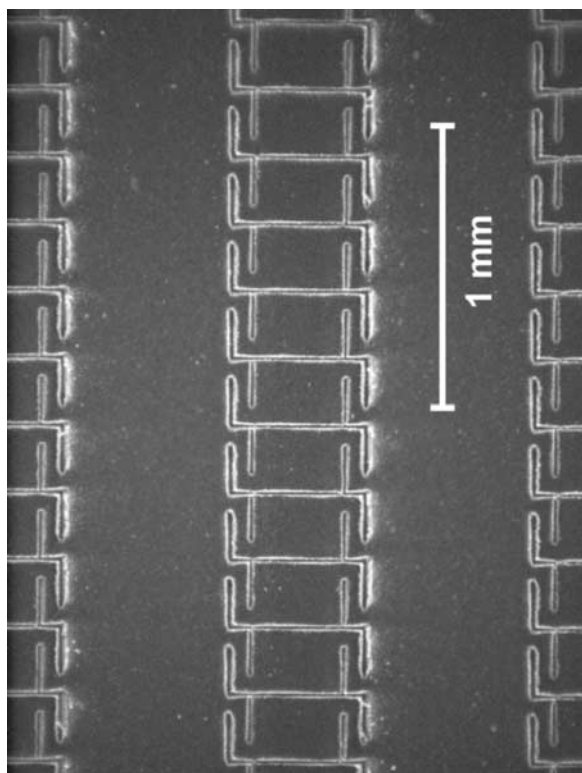


**Figure 7.** MCS thermopile detector array coated with gold black.

necessary to remove the few remaining gold black bridges using a focused ion beam. An MCS detector array is shown in Figure 7 after gold black deposition and laser and ion beam ablation.

[32] The MCS observation cycle consists of two-second signal integration intervals, interspersed every 34 seconds with instrument views of space. This corresponds to a 0.03 to 0.25 Hz frequency range. Thus low  $1/f$  noise in both the detectors and the readout circuitry is essential. Thermopile detectors intrinsically have low  $1/f$  noise because when read out with high-input-impedance voltage amplifiers they exhibit negligible current flow. Each group of 64 detector pixels is read out with a custom CMOS readout integrated circuit. The architecture of this circuit is shown in Figure 8. A readout chip is connected to each thermopile array with two wire bonds per detector pixel. The roughly DC signal from each pixel is modulated at 64 kHz by an electronic chopping circuit. The resulting AC signal is amplified, demodulated, and integrated. Because amplification occurs at 64 kHz rather than near DC, the  $1/f$  noise in the CMOS amplifier is dramatically reduced. Integrated signals from 64 channels are multiplexed into a single analog output stream.

[33] Thermopile detector noise is dominated by Johnson noise, which, for the  $100\text{ k}\Omega$  MCS detectors, is  $40\text{ nV/Hz}^{1/2}$ . With a  $100\text{ k}\Omega$  source, the readout chip has an input-referred noise of  $70\text{ nV/Hz}^{1/2}$  for 0.03 to 0.25 Hz. Thus the readout chip is the dominant focal plane noise source. Even with this readout noise, the MCS focal planes demonstrate  $D^*$  values of  $8 \times 10^8\text{ cmHz}^{1/2}/\text{W}$  for 0.03 to 0.25 Hz.

### 3.5. Mechanisms

[34] The instrument FOV can be directed over the full operating range of  $270^\circ$  in azimuth and elevation by stepper motor actuators. Twist capsule assemblies for each axis contain the stepper motors, gearing, position sensing diodes, and flexible leads.

[35] Both motors are brushless stepper motors with a step size of  $30^\circ$ , geared down by a factor of 297:1 by planetary gears and harmonic drives in series. The resulting step size granularity for instrument rotation is  $0.1^\circ$ , or half the vertical instrument FOV at the limb of Mars, which corresponds to roughly one quarter of the atmospheric scale height (the scale-height is  $\sim 10\text{ km}$ ). Encoders are not used. Instead, diodes coupled with drive phase information define two reference positions and software checks for inconsistencies between commanded and reference positions. If inconsistencies are detected, motor positions are re-initialized. Flexible leads within the twist capsule assemblies supply data, signal, and power connections between the OBA, the yoke, and the spacecraft across the moving interfaces.

[36] The motors are driven open loop by electronics in the yoke controlled by software. In order to minimize mean torque and jitter, and the possibility of induced disturbance of the spacecraft, instrument slews are divided into constant acceleration, constant velocity, and constant deceleration phases. The drive waveforms are micro-stepped to smooth the low frequency jitter produced by individual steps. Drive voltage and phase information that can be used to generate slews are stored in uploaded azimuth and elevation slew tables in MCS memory. The slew tables specify accelerations and decelerations of  $25^\circ/\text{s}^2$  in azimuth and  $42^\circ/\text{s}^2$  in elevation with a top speed of  $26.5^\circ/\text{s}$  in both axes.

[37] A complete flight spare actuator assembly was used to perform accelerated life testing of the MCS actuators over  $3.5 \times 10^6$  measurement cycles, or  $5.2 \times 10^8$  motor revolutions. For the purposes of the test, a cycle consists of two opposite  $90^\circ$  slews. This represents a factor of two margin over the total anticipated elevation actuator motions during the nominal MRO mission of one Mars year. The life test was made more conservative by combining the higher number of elevation actuator cycles with the larger azimuth actuator mechanical load at cold ( $-5^\circ\text{C}$ ), warm ( $20^\circ\text{C}$ ), and hot ( $50^\circ\text{C}$ ) operating temperature plateaus. The life test finished successfully in March 2006, and the actuator is now being disassembled and inspected for wear.

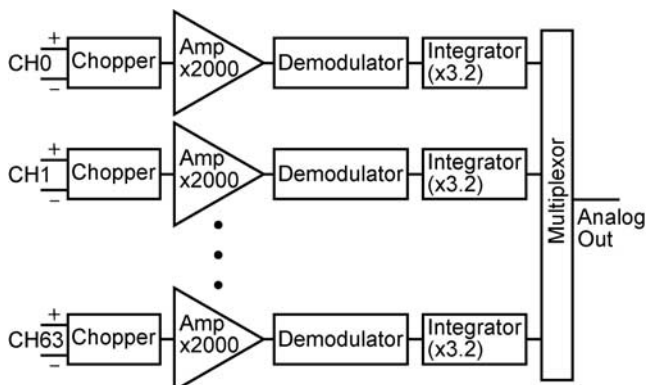


**Figure 8.** Architecture of focal plane readout integrated circuit.



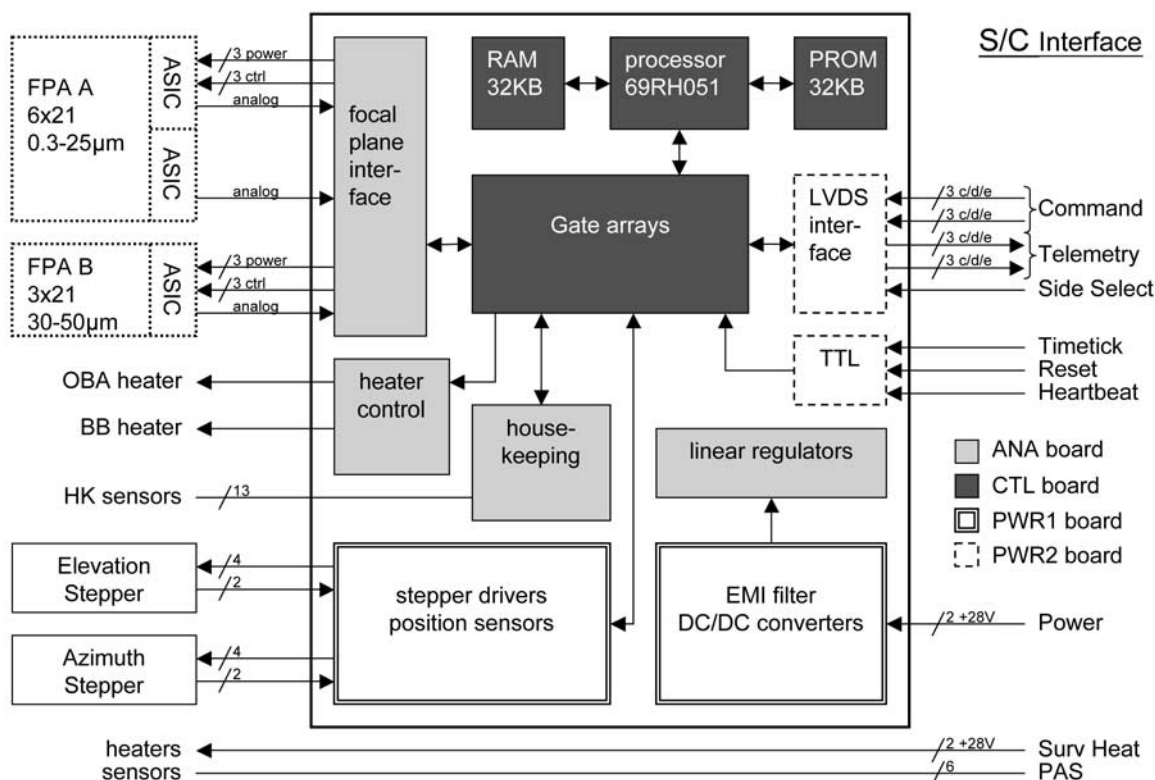


Figure 9. MCS electronics functional block diagram.

### 3.6. Electronics and Software

[38] The main elements of the MCS electronics are shown in the functional block diagram of Figure 9. The diagram is color-coded to denote the location of the elements on the analog, control, and power boards. The analog board accommodates analog signal processing electronics and the control board contains digital controller electronics. These boards are mounted on opposite sides of the OBA to minimize mutual interference. The power boards are mounted on the yoke, to isolate them from the other boards, and accommodate power conditioning, actuator driver, and spacecraft interface electronics.

[39] The core of the MCS electronics is the digital controller, comprising a processor coupled with 32 kBytes of RAM, 32 kBytes of ROM and a FPGA. Its primary functions are as follows:

- [40] 1. Control focal plane readout integrated circuits and digitize, collect, and process signals.
- [41] 2. Provide set-points and variable heater power for the optical bench and blackbody targets.
- [42] 3. Control housekeeping data sampling, collection, and process housekeeping data.
- [43] 4. Control the actuators.
- [44] 5. Receive and process spacecraft commands.
- [45] 6. Generate telemetry packets and transmit them to the spacecraft.
- [46] 7. Provide DC/DC converter synchronization and the 31.25 Hz real-time clock.
- [47] The focal plane interface electronics digitizes the multiplexed integrated analog signals from the three 64-channel readout integrated circuit chips on the two MCS focal planes. All 192 signals are sampled at 1 kHz, and 2048 samples are

digitally integrated by the FPGA resulting in an effective signal integration period of 2.048 seconds.

### 3.7. In-Flight Calibration

[48] MCS performs a two-point in-flight radiometric calibration of its signals, to correct for the effects of thermal drifts, using views of space and of calibration targets mounted on the instrument yoke (Figure 1). Views of space, accomplished by using the elevation actuator to slew the instrument above the limb, provide a zero reference for all MCS spectral channels. Space views are obtained at 34-second intervals during standard limb viewing observations.

[49] A second calibration point is supplied for the infrared channels by rotating the instrument so that the blackbody target in the yoke fills the aperture and FOV of both telescopes. The telescopes are directed toward the target approximately 10 times per orbit using the elevation actuator. In order to meet the MCS absolute radiometric calibration requirement of better than  $\pm 0.5\%$  at 300 K, the target must be thermally uniform, and its temperature and emissivity known with an accuracy of better than  $\pm 0.25$  K and  $\pm 0.0035$ , respectively. The required temperature and emissivity accuracies are met using a grooved aluminum plate, blackened by the Martin Black anodize process. Target temperature is monitored by two platinum resistance thermometers embedded at the center of each viewed area of the plate. One sensor is used to control the target temperature via a distributed heating element on the rear surface of the target. MCS is designed so that the blackbody target is mounted very close to the telescope apertures. Controlling the target temperature within a few degrees of

the telescope temperature compensates, in part, for non-zero reflectivity of the target surface.

[50] For the visible channel, a second calibration point is provided by the solar target that fills the aperture of telescope A. Telescope A is rotated to view the solar target twice per orbit as the sun rises or sets over the limb of Mars. The sun is at an angle of roughly  $15^\circ$  below the local horizontal for these measurements. The solar target diffusively scatters solar radiation into the telescope. In order to meet an absolute radiometric calibration requirement of better than  $\pm 3\%$ , the target reflectivity must be nearly Lambertian. The target was characterized before launch over the expected range of viewing and illumination angles. It is also critical that the target surface reflectivity not change significantly over the lifetime of the mission. A textured aluminum target plate is suspended within and thermally isolated from a supporting base structure. A means of self calibration of the target is included in its design. In the configuration used here, the target and base form a calorimeter. Monitoring the target and base temperatures when the target is heated by the sun provides a direct indication of any changes in reflectivity during the mission. Corrections can then be applied to the instrument calibration measurements.

[51] During spacecraft system thermal vacuum testing, the MCS solar target was exposed to potential contamination by organics. This raised the question of whether the target might change, most probably darken, when exposed to solar UV radiation in space. The MRO spacecraft was configured during cruise to enable the MCS team to conduct two previously unscheduled tests of the solar target. These tests permitted a two-point intercomparison of target reflectivity after a total of 40–50 hours of exposure to the sun. Analysis of the test data demonstrated that any change in target reflectance is less than 0.1%.

#### 4. Observation Strategy

[52] The observation strategy employed by MCS performs (limited by intermittent off-nadir pointing by MRO in support of HiRISE, CRISM and CTX [Zurek and Smrekar, 2007]) uninterrupted repetitive measurements over the life of the mission. Minimizing gaps in limb sounding is consistent with our objective to accumulate a climatology of Mars. MCS performs repetitive observations autonomously, utilizing an internal table-drive scheme that is loosely keyed to the spacecraft's latitude. The planet's aspheric shape and MRO orbital eccentricity are sufficient to require latitude-dependent, although not longitudinal, adjustments to MCS pointing for limb-staring observations.

[53] The near-polar orbit enables MCS to use the descending (night side) equator crossing to synchronize its observations with spacecraft latitude. Ephemeris routines onboard the spacecraft are used to generate a command containing equator-crossing time that is transmitted to MCS every orbit. The acceptable error in equator-crossing time is 10 seconds. If equator-crossing time is not received by MCS, the instrument extrapolates from earlier equator-crossing times.

[54] Articulation of MCS, and thus its pointing direction, is controlled by three sets of nested tables through which instrument software loops repetitively. Running at a top

level is the Orbit Schedule Table (OST) that determines which of three Event Schedule Tables (EST) is to be used from orbit to orbit. The EST controls all activities over the course of an orbit and contains a list of calls to Scan Sequence Tables (SST) ordered by time relative to the last equator crossing. An SST describes a small, frequently used scan pattern, such as a limb view or a calibration cycle, and consists of a list of scanning instructions including which axis to scan, where to go, and how many soundings to acquire at that destination. When an SST completes, software determines whether to call it again or move on to the next SST, based on time since the last equator crossing in the EST. Each SST normally executes to completion so that some orbit-to-orbit variability in timing is introduced. Two other tables also modify observations round the orbit. An Elevation and Oblateness Correction Table (EOCT) contains a list of elevation step perturbations, again ordered by time relative to the last equator crossing. This table allows selected SSTs, such as a limb view, to be perturbed to track the limb by correcting for the MRO orbit and the oblateness of Mars. Finally, a Radio Occultation Table (ROT) contains the time and geometrical information needed to perturb a limb view so that it views the limb where and when the Earth is rising or setting through it (see section 4.3).

[55] Default scan tables retained in MCS memory are utilized by instrument software if alternates are not uploaded following instrument turn on. Default SSTs enable limb viewing, with approximations for orbit eccentricity, to retrieve vertical profiles of temperature, dust, water, and condensates. These default tables also include SSTs unique to the polar regions where MCS performs so-called “buckshot” observations: varying the angle of observation of the upward going radiation. Prescribed “buckshot” patterns provide optimized coverage of the bi-directional reflectance function (BDRF) of the polar caps for determining the polar energy balance in the north and south. MCS also performs limb observations in the polar regions to provide nearly continuous atmospheric profiling. Default scan tables can be replaced by uploads from Earth to accommodate orbit changes, seasonal variations, changes in observational strategies, and correlative observations with other instruments or the MRO spacecraft. Table loads have already been used in flight to facilitate MCS checkouts during the cruise, including performing solar target calibration tests and characterizing potential interactions among payload elements, e.g., instrument motion-induced disturbances.

[56] MCS performed anomaly free during the cruise to Mars and in tests in the initial capture orbit. In section 5, we show an early demonstration that the instrument is functioning properly with data collected soon after MRO capture into orbit about Mars.

##### 4.1. Observations of the Atmosphere at the Limb

[57] The design of the actuators allows MCS to view the limb of the atmosphere in any direction from the spacecraft. We have elected to use the forward in-track limb in the direction of the spacecraft velocity vector to take advantage of the overlap of limb and nadir measurements, and the line-of-sight overlap in successive vertical profiles of the atmosphere. In addition, the fore and aft limb directions are the least at risk for accidental direct views of the sun. The

buckshot observation is also much more efficient when combined with forward limb views.

[58] The MCS limb profiling sequence involves three different viewing directions. The first is a view of the surface at nadir directly below the spacecraft for four seconds, or two measurement integration intervals. The second is a view of the forward limb for 16 seconds, and the third is a view of space above the limb for four seconds. The latter view is used to calibrate the other observations, providing slow chopping between the scene and space. In the nominal limb sequence, the instrument repeats this three-step pattern every 34 seconds, when the time required to move from one view to the next is included, so that atmospheric profiles are acquired every 110 km or  $1.86^\circ$  in latitude. The nadir view is combined with the limb view of the “same” atmosphere taken earlier in the orbit to improve the retrieval of near-surface atmospheric properties. As part of the nominal in-track limb view sequence, MCS will obtain nadir measurements of emitted surface infrared radiance and broadband solar reflectance.

[59] Although in-track is the default observing mode for MCS, cross-track limb observations will be made with the same vertical resolution in order to obtain coverage of local time of day variability in the atmosphere. The cross-track limb is approximately 1.5 hours ahead (behind) the local time of the in-track limb at the equator. Time of day coverage increases poleward and is complete at  $\pm 67^\circ$  latitude.

#### 4.2. Polar Observations

[60] In the polar regions, MCS will employ buckshot scanning sequences. The combined daily geometric coverage is shown in Figure 11. The intention of these off-nadir observations is to characterize the angular dependence of reflected and emitted radiation at the top of the atmosphere. The ability of MCS to point in any direction beneath the spacecraft will enable much more complete measurements of the Martian polar radiative balance than have been possible to date. In buckshot mode, observations are arranged in concentric circles to sample emission angles while also providing geographic coverage. The pattern is then repeated to cover the polar ice cap.

[61] Buckshot observations will also improve the characterization of diurnal and seasonal temperature variations to determine surface and subsurface bulk thermal properties for estimating the distribution of near-surface ground ice [Paige *et al.*, 1994; Paige and Keegan, 1994].

#### 4.3. Coincident Line of Sight Measurements With Radio Science

[62] MCS has inherited from the PMIRR operations architecture the ability to perform coincident observations with spacecraft radio occultation opportunities. When activating this observation scheme, the ROT table replaces ongoing activities at the appropriate time in the orbit and performs a limb observation in the direction of a predicted occultation of the Martian atmosphere between MRO and Earth. The vertical detector arrays provide profiles comparable, although with lower resolution, to those obtained from the radio signal. However, there is no MRO science team to make use of the radio occultation data. Consequently, MCS may not be able to take advantage of these opportunities. The MGS mission has made excellent use of its

infrared spectrometer and radio science experiments for data validation and calibration [e.g., Hinson *et al.*, 2004; Montabone *et al.*, 2006].

#### 4.4. Accommodations for Spacecraft Off-Nadir Pointing and Periods of High-Resolution Imaging

[63] A nadir-fixed platform is preferred by MCS. However, other elements of the MRO payload require the spacecraft to roll its nadir pointing orientation by as much as  $30^\circ$ . Roll angles of less than  $9^\circ$  can be accommodated using the two detector margin at the top and bottom of the vertical profile. However, when the angle of spacecraft roll exceeds about  $9^\circ$ , the MCS detector arrays no longer cover the entire vertical range of atmosphere (0 to 80 km) in the forward limb view. Consequently, the MRO Project Science Group (the formal group comprising the payload Principal Investigators) has undertaken to limit requests for large rolls greater than  $9^\circ$ . This compromise is possible because, with planning, most surface targets can be viewed within 30 days using spacecraft roll angles less than  $9^\circ$ . Were these practices not acceptable to the other MRO instrument teams, more frequent gores in MCS data would have seriously compromised the climatology record.

[64] HiRISE will obtain a number of stereo images requiring the spacecraft to perform, on average, one large roll per stereo pair. These observations will disrupt the continuity of MCS measurements over a period of 15 minutes, or  $48^\circ$  in latitude. To mitigate this problem and reduce the number and extent of incomplete vertical profiles, MCS can be commanded to react to rolls larger than  $9^\circ$  by changing its nominal observing pattern. In these cases, MCS alternates its FOV between two positions that together overlap covering the desired 0- to 80-km altitude range. Data taking will proceed through all roll events and calibrated radiances will be flagged and archived.

[65] In addition to disruptions due to spacecraft rolls, the HiRISE instrument needs a quiet platform from which to obtain its highest-resolution images. Ground testing indicates that MCS-induced spacecraft jitter exceeds permitted levels when either azimuth or elevation actuators are operated. Therefore, through a signal sent from the spacecraft to MCS the instrument will be commanded to “Freeze” for the duration of high-resolution imaging. In Freeze mode, MCS moves to view the limb and then remains stationary for 60–90 seconds when it is then commanded to return to routine activities.

#### 4.5. Expected Spatial and Temporal Coverage of Mars

[66] The MRO spacecraft uses a frozen orbit during the primary science phase of the mission, with a planned periapsis altitude of 255 km at the south pole, an apoapsis altitude of 320 km at the north pole, and an orbital period of 112 minutes, 12 seconds. The orbit inclination of  $92.6^\circ$  is chosen to give full latitudinal coverage and assure a nominal solar-fixed dayside equator crossing time of 3:00 pm by matching the orbit precession rate to the mean angular velocity of Mars around the Sun.

[67] The latitudinally dependent pattern of MCS observations begins each night-side descending equator crossing, as discussed above. Figure 10 shows the coverage, in rectangular coordinates, of Mars obtained by MCS in



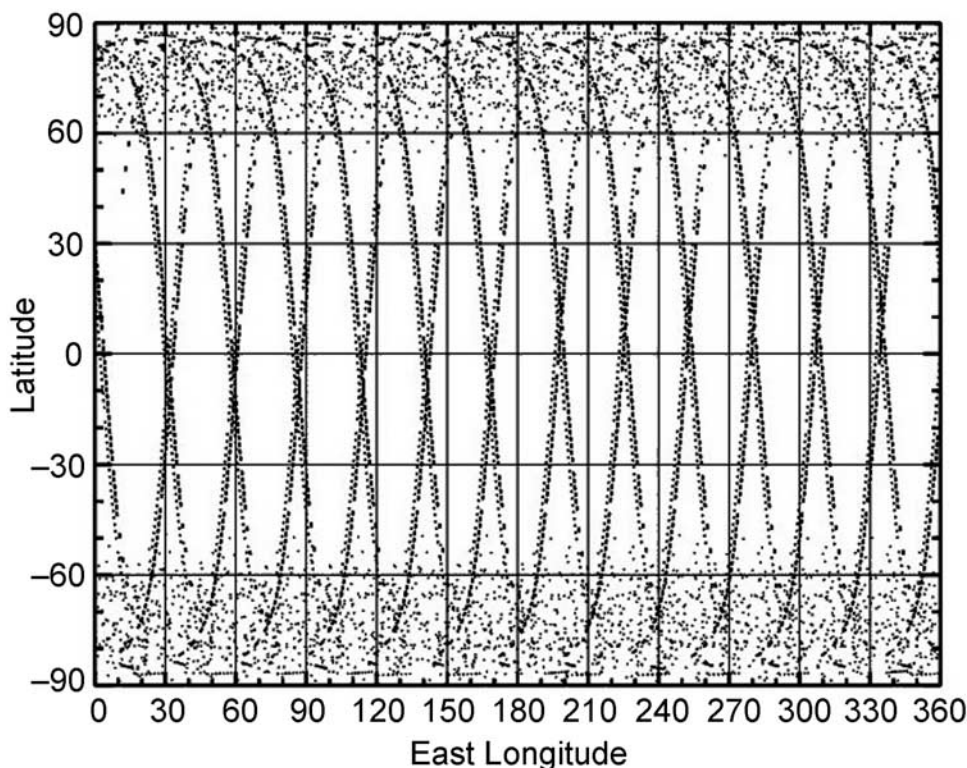


**Figure 10.** Mercator projection of 24 hours of MCS spatial coverage. Each science observation is plotted as a point, either on the surface for surface views or at the location of the tangent point of the array for limb observations. The group of 8 limb observations for each limb view appears as a dash due to the spacecraft motion during their acquisition. The ascending (or day side) tracks slant from the lower right to upper left, while the descending (or night side) tracks slant the opposite direction.

approximately one day of default operations. Figure 11 shows the coverage to  $60^\circ$  latitude in polar coordinates.

[68] Close inspection of Figure 10 shows regularly spaced gaps due to calibration measurements. MCS limb observations have a latitudinal spacing of 110 km ( $1.86^\circ$ ) and an orbit-to-orbit longitudinal spacing of  $27^\circ$ , determined by the rotation of Mars. Limb measurements are made less frequently at high latitudes to accommodate buckshot observations. However, the convergence of orbit spacing near the poles compensates for less frequent sampling of the limb.

## 5. Instrument Testing, Characterization, and Calibration

[69] MCS was operated in a stand-alone configuration under laboratory thermal-vacuum conditions for approximately 500 hours. During this time, extensive pre-flight calibration was performed. Radiometric calibration was accomplished using external high-emissivity blackbody targets controlled and monitored at temperatures extending over the full range of Martian conditions, as well as simulations of deep space. Detector linearity was measured for all elements in the linear arrays. The internal instrument blackbody target located in the yoke was calibrated. Channel electronic gain and offsets were established. Electronic offsets are determined at Mars every ten minutes by viewing the internal blackbody and space. The FOVs of all detectors were measured using a target projector, and their spectral response was determined using a monochromator, both

within the thermal vacuum test chamber. Figure 12 shows the spectral response of detector 11 of the thermal channels obtained during thermal vacuum characterization of MCS.

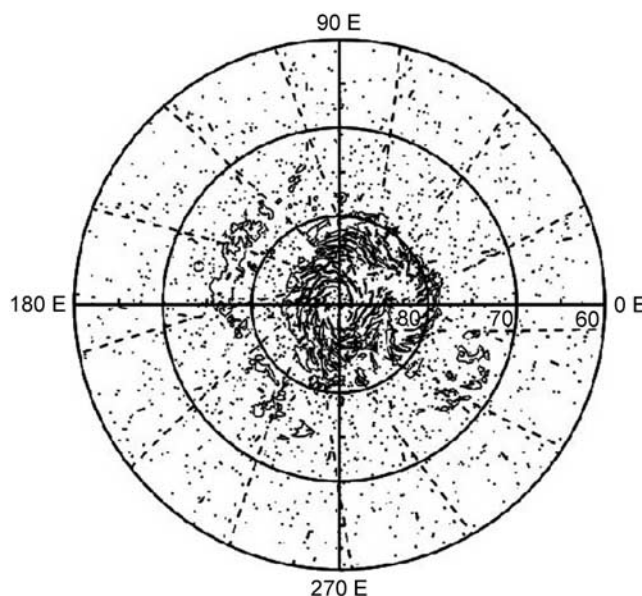


**Figure 11.** North polar projection of 24 hours of MCS spatial coverage. The observations are plotted as in Figure 10, except to only  $60^\circ$  latitude.

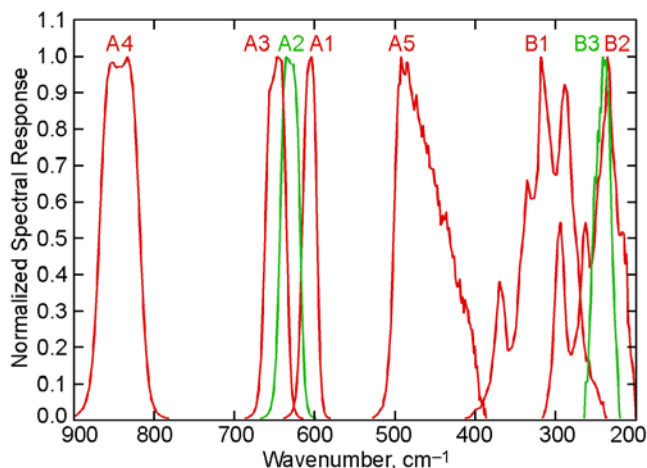


**Figure 12.** Normalized measured response of MCS thermal spectral channels.

[70] Limited testing of MCS has been performed in Mars orbit. On 25 March 2006, near apoapsis of the elliptical capture orbit, tables were up loaded and the instrument scanned Mars. The primary purpose of collecting scans of the planet was to demonstrate the capability of the MCS to support aerobraking planning, should it be needed. Figure 13 shows images of Mars in 8 of the 9 spectral channels, derived from a raster scan of the planet. Over a period of half an hour, the MCS detector arrays were scanned across the planet, producing the images in the figure. Looking down on the northern hemisphere, the early spring polar CO<sub>2</sub> cap is visible in the center left of each image. These data are also being used by the team to validate the ground calibration of FOVs.

## 6. Data Analysis, Interpretation, and Modeling

[71] In this section, we describe the application of MCS measured radiances to investigations of the weather and climate of Mars. The areas of research discussed below are the primary focus of the MCS science team. Due to resource limitations, delivery of standard MCS data products to the Planetary Data System (PDS) Atmospheres Node [McMahon, 1996] within 6 months following the receipt of data on the ground will be limited to Experimental Data Records (EDRs) (Level 0 unpacked data products) and Reduced Data Records (RDRs) (Level 1 calibrated radiances along with viewing geometry information). However, over the course of the mission, Derived Data Records (DDR) in the form of Level 2 data products (retrieved geophysical profiles) created by the MCS team will be archived with the PDS within 18 months of the receipt of data. Specialized data products, consisting of images and maps of atmospheric and surface fields produced by the team, will be delivered to PDS on a best-effort basis.

### 6.1. Thermal Structure, Amounts of Dust and Condensates, and Water Vapor Abundance

[72] Central to the MCS investigation is the development of a climatology of atmospheric parameters, including temperature, the optical depth of dust and condensates of H<sub>2</sub>O and CO<sub>2</sub>, and the amount of water vapor, all in vertical profiles. McCleese *et al.* [1992] developed retrieval tools for these quantities based upon the techniques of Chahine [1970]. More recently, a complementary approach utilizing the retrieval approach of Rodgers [1976] has been developed by the team. In the latter case, retrieval schemes that were originally developed and used in Earth and outer planet applications are now modified for Mars application.

[73] Mars climatology developed from measurements made by instruments on earlier missions lacks the vertical

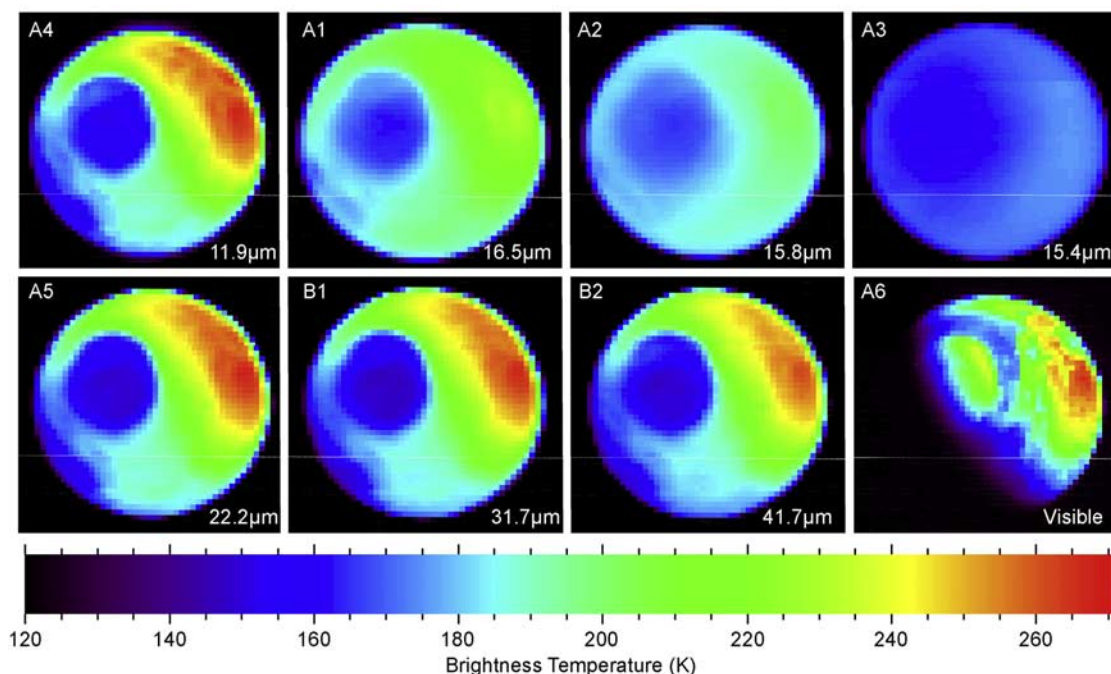


**Figure 13.** Aerobraking support demonstration images in eight MCS spectral channels.



resolution and altitude coverage needed to explore fully the forcing mechanisms for the circulation of the Martian atmosphere. They also lack a resolved vertical structure of suspended dust, water vapor and clouds. Numerical model experiments have been found to be sensitive to all of these parameters. Specifically, suspended dust is a highly variable component of the atmosphere that can greatly modify the vertical (and horizontal) thermal structure of the atmosphere and contribute to complex feedbacks involving adiabatic heating of the airborne dust and its transport by the atmosphere. In addition to the total airborne dust content observed previously, MCS will resolve its vertical structure, which has been shown to influence strongly the circulation. Also, much of the observed interannual, seasonal, and shorter-term variability of the atmospheric circulation is known to be a consequence of dust lifted from the surface by wind. The dust lifting processes have no close analogs on Earth, yet it is a goal to include them in general circulation models.

[74] Infrared sounding of the Martian atmosphere is also made more difficult by extinction, emission and scattering by suspended dust. Retrieval of variable atmospheric constituents, e.g., water vapor, from infrared soundings depends upon discriminating between radiances arising from airborne dust in the line of-sight and that emitted by the species of interest, e.g., CO<sub>2</sub>. The work of *Bandfield and Smith* [2003] in obtaining the spectral properties of the airborne dust from TES nadir observations will be critical to MCS retrievals in these instances. This information will enable the use of MCS radiance ratios near 12, 22, 32 and 42  $\mu\text{m}$  (see Table 2) to distinguish dust, CO<sub>2</sub>, water vapor and condensates. TES data shows indications of subtle changes in the dust spectral shape attributed to particle size changes [*Wolff and Clancy*, 2003] that appear to be associated primarily with dust storms, but also have a seasonal dependence [*Clancy et al.*, 2003]. We are not aware of any detailed analysis of TES limb data for altitude-dependent dust properties. The TES retrievals ignore these climatological changes, having determined they introduce negligible errors [*Smith*, 2004]. Scattering by dust is also important in retrieving temperature and constituents near the surface of Mars where emitted radiance from the surface and adjacent layers can be scattered into the instrument FOV. The final climatological record resulting from MCS will accommodate these complexities.

[75] The MCS design includes two channels, B3 (230–245  $\text{cm}^{-1}$ ) and B2 (220–260  $\text{cm}^{-1}$ ), for the retrieval of water vapor. B3 is a narrow channel located between two strong water vapor absorption features, while B2 is a broader channel that includes both of these features. As the two channels are centered at similar wavelengths, they have similar sensitivities to dust but quite different sensitivities to water vapor, in principle allowing water mixing ratio and dust extinction to be retrieved simultaneously, given separate information on the temperature profile. However, while the mesh filters for the B-channels met specifications when measured separately following their manufacture, it was discovered when characterizing the flight instrument that the spectral response in these channels had changed. Some mesh filter channels had broadened significantly and showed significant variations from detec-

tor to detector within an array. The cause is still to be explored fully.

[76] With the final filter profiles (Figure 12), including a B3 channel that is much broader than intended, the performance of MCS for retrieving water vapor using the method outlined above is compromised. The sensitivity of individual channels to water vapor is not affected, but using the radiance ratio B3/B2 to reduce the sensitivity to dust opacity now eliminates most of the sensitivity to water also. An alternative approach that combines B2 and B3 measurements with those of B1 and A5 is being developed. An anticipated weakness of this approach is that the separation of the channels is now such that the spectral characteristics of dust must be provided from other sources, such as TES climatology (see above), or empirically from MCS limb radiances. The consequent increase in the error budget of the water measurements from MCS will be established in due course by sensitivity studies.

## 6.2. Atmospheric Circulation, Transport of Dust and Water, and Interannual Variability

[77] Data assimilation, the integrating of observations into a general circulation model of the Martian atmosphere with a meteorological assimilation scheme, has the advantage of deriving atmospheric properties not measured directly by the instrument (including inevitable observational gaps, see above). Long term, we anticipate assimilating MCS retrieved temperatures and dust opacities into the extended version of the *Forget et al.* [1999] Mars GCM model using the assimilation scheme developed by *Lewis and Read* [1995] and refined by *Lewis et al.* [1996, 1997] and S. R. Lewis et al. (Assimilation of thermal emission spectrometer atmospheric data during the Mars Global Surveyor aerobraking period, submitted to *Icarus*, 2006; hereinafter referred to as *Lewis et al.*, submitted manuscript, 2006) to obtain a detailed and continuous synoptic analysis of the complete state of the Martian atmosphere for the duration of the MRO mission. Eventually, retrieved profiles of temperature, dust and water vapor will be used to guide the model and obtain estimates of the fully 3D time-dependent state of all model atmospheric parameters. This will help isolate and correct model biases and, in due course, the assimilation results will be analyzed for the transport of both dust and water (as vapor and as ice). Other long term goals supported by assimilation include quantifying the role of dynamical processes in the atmosphere as a function of season, location, and dust loading, evaluating the predictability of weather systems in the Martian atmosphere, and quantifying various processes (including dust storm initiation and decay) in the transport cycles of dust and water. Comparisons with a similar analysis of data from TES [e.g., *Lewis and Barker*, 2005; *Montabone et al.*, 2005; *Lewis et al.*, submitted manuscript, 2006] will help to evaluate interannual climate variability on Mars. Of particular interest are the variability in baroclinic storm activity and changes in storm tracks correlated, potentially, with dust or cloud amounts and their vertical distributions.

## 6.3. Polar Radiative Balance

[78] Measurements of the radiative balance of the Martian polar caps provide strong constraints on the behavior Mars' present CO<sub>2</sub> cycle, as well as insights into processes that



may be important for climatic change. The current behavior of CO<sub>2</sub> frost on Mars is asymmetric: the residual cap in the north is composed of water ice, whereas the residual cap in the south appears to be composed partially of CO<sub>2</sub>. *Paige and Ingersoll* [1985] used Viking Infrared Thermal Mapper (IRTM) observations to determine the annual radiation balance at the Martian north and south residual caps, and concluded that the survival of seasonal CO<sub>2</sub> in the south is made possible by its high albedo. This asymmetry may be a natural consequence of competition for CO<sub>2</sub> between the north and south residual caps [*Palluconi and Kieffer*, 1979], and the reinforcing effects of subsurface heat conduction in the exposed north polar water ice cap [*Jakosky and Haberle*, 1990]. New remote sensing data for the south residual polar cap reveal varied textures [*Thomas and Weitz*, 1989] and the existence of substantial quantities of water ice [*Titus et al.*, 2003; *Bibring et al.*, 2004], suggesting a complex recent volatile history. Images obtained one Mars year apart show substantial interannual variations in the fine-scale morphology of the surface of the south residual cap, and suggest that the CO<sub>2</sub> frost cover may be disappearing rapidly under current climatic conditions.

[79] MCS will measure the polar radiation balance using an approach similar to that employed previously for the Viking IRTM observations [*Paige and Ingersoll*, 1985]. MCS solar channel radiances will be used to determine net absorption of solar radiation below the top of the atmosphere and MCS thermal infrared radiances will be used to determine the net upward flux of infrared radiation at the top of the atmosphere. The enhanced MCS polar spatial and temporal coverage, compared with previous observations, will enable polar radiative balance measurements to be conducted not just at the locations of the residual polar caps, but in all regions poleward of  $\sim 70^\circ$  latitude. The results of these observations should make it possible to define the properties and processes that control the annual CO<sub>2</sub> cycle in the Martian polar regions, and provide insight to mechanisms that may be responsible for climatic change on Mars.

## 7. Summary

[80] The Mars Climate Sounder will be the first custom-designed infrared sounder for systematic meteorological measurements at Mars, using the limb viewing technique to obtain relatively high vertical resolution of better than one pressure scale height. Its deployment is long overdue, because of the failures with Mars Observer and Mars Climate Orbiter in 1993 and 1999 respectively, but the delay has allowed the application of modern technology to give a more compact and versatile design. In particular, the use of new high performance, linear array thermopile detectors with focal plane signal processing and miniature multilayer interference and mesh filters has permitted a five-fold reduction in mass, in part by the elimination of the requirement for cryogenic operation of the focal plane.

[81] The compact dimensions of the design allow the entire instrument to be pointed to limb or nadir, for atmospheric and surface mapping respectively, and special patterns to be implemented, for example for mapping over the poles where the complex physics of the energy balance and atmospheric response during the long winter night is to

be addressed. Plans are in hand to assimilate the global temperature, dust and water vapor profiles into sophisticated general circulation models of the atmosphere as an efficient means of data interpretation and to provide new tools for studying past and future climate scenarios, as well as better understanding the present [*Taylor et al.*, 2006]. These models are also expected to be invaluable when planning and implementing new missions to the surface of Mars, particularly those with high-mass payloads that are extremely sensitive to meteorological conditions encountered during entry, descent and landing.

[82] **Acknowledgment.** This work was carried out at the Jet Propulsion Laboratory, California Institute of Technology.

## References

- Bandfield, J. L., and M. D. Smith (2003), Multiple emission angle surface-atmosphere separations of Thermal Emission Spectrometer data, *Icarus*, **161**(1), 47–65.
- Bibring, J.-P., et al. (2004), Perennial water ice identified in the south polar cap of Mars, *Nature*, **428**, 627–630.
- Boynton, W. V., et al. (2002), Distribution of hydrogen in the near surface of Mars: Evidence for subsurface ice deposits, *Science*, **297**(5578), 81–85.
- Cantor, B., M. Malin, and K. S. Edgett (2002), Multiyear Mars Orbiter Camera (MOC) observations of repeated Martian weather phenomena during the northern summer season, *J. Geophys. Res.*, **107**(E3), 5014, doi:10.1029/2001JE001588.
- Chahine, M. T. (1970), Inverse problems in radiative transfer: Determination of atmospheric parameters, *J. Atmos. Sci.*, **27**, 960–967.
- Christensen, P. R., et al. (2001), Mars Global Surveyor Thermal Emission Spectrometer experiment: Investigation description and surface science results, *J. Geophys. Res.*, **106**(E10), 23,823–23,872.
- Clancy, R. T., M. J. Wolff, and P. R. Christensen (2003), Mars aerosol studies with the MGS TES emission phase function observations: Optical depths, particle sizes, and ice cloud types versus latitude and solar longitude, *J. Geophys. Res.*, **108**(E9), 5098, doi:10.1029/2003JE002058.
- Farmer, C. B., D. W. Davies, A. L. Holland, D. D. LaPorte, and P. E. Doms (1979), Mars: Water vapor observations from the Viking orbiters, *J. Geophys. Res.*, **84**, 2881–2888.
- Foote, M. C., E. W. Jones, and T. Caillat (1998), Uncooled thermopile infrared detector linear arrays with detectivity greater than  $10^9$  cm Hz<sup>1/2</sup>/W, *IEEE Trans. Electron Devices*, **45**, 1896–1902.
- Foote, M. C., M. Kenyon, T. R. Krueger, T. A. McCann, R. Chacon, E. W. Jones, M. R. Dickie, J. T. Schofield, D. J. McCleese, S. Gaalema, and W. Hu (2003), Thermopile detector arrays for space science applications, paper presented at International Workshop on Thermal Detectors for Space Based Planetary, Solar, and Earth Science Applications (TDW), NASA, Adelphi, Md. (Available at <http://www-lep.gsfc.nasa.gov/code693/tdw03/proceedings/docs/s2.html>)
- Forget, F., F. Hourdin, R. Fournier, C. Hourdin, O. Talagrand, M. Collins, S. R. Lewis, P. L. Read, and J. P. Huot (1999), Improved general circulation models of the Martian atmosphere from the surface to above 80 km, *J. Geophys. Res.*, **104**(E10), 24,155–24,175.
- Formisano, V., et al. (2005), The Planetary Fourier Spectrometer (PFS) onboard the European Mars Express mission, *Planet. Space Sci.*, **53**(10), 963–974.
- Hanel, R. B., B. Conrath, W. Hovis, V. Kunde, P. Lowman, W. Maguire, J. Pearl, J. Pirraglia, C. Prabhakara, and B. Schlachman (1972), Investigation of the Martian environment by infrared spectroscopy on Mariner 9, *Icarus*, **17**, 423–442.
- Hawkins, G. J., and R. Hunneman (1994), Design and fabrication of infrared filters for remote sounding instrumentation, *Proc. SPIE Int. Soc. Opt. Eng.*, **2210**, 639–651.
- Hess, S. L., R. M. Henry, C. B. Leovy, J. E. Tillman, and J. A. Ryan (1977), Meteorological results from the surface of Mars: Viking 1 and 2, *J. Geophys. Res.*, **82**, 4559–4574.
- Hinson, D. P., M. D. Smith, and B. J. Conrath (2004), Comparison of atmospheric temperatures obtained through infrared sounding and radio occultation by Mars Global Surveyor, *J. Geophys. Res.*, **109**, E12002, doi:10.1029/2004JE002344.
- Houghton, J. T., and F. W. Taylor (1973), Remote sensing of the atmospheres of the Earth and planets from satellites and spacecraft, *Rep. Prog. Phys.*, **36**(7), 827–919.
- Irwin, P. G. J., P. A. R. Ade, S. B. Calcutt, F. W. Taylor, J. S. Seeley, R. Hunneman, and L. Walton (1993), Investigation of dielectric spaced resonant mesh filter designs for PMIRR, *Infrared Phys.*, **34**, 549–563.

- Jakosky, B. M., and C. B. Farmer (1982), The seasonal and global behavior of water vapor in the Mars atmosphere: Complete global results of the Viking atmospheric water detector experiment, *J. Geophys. Res.*, **87**, 2999–3019.
- Jakosky, B. M., and R. M. Haberle (1990), Year to year instability of the Mars south polar cap, *J. Geophys. Res.*, **95**, 1359–1365.
- Laskar, J., and P. Robutel (1993), The chaotic obliquity of the planets, *Nature*, **361**, 608–612.
- Leovy, C. (2001), Weather and climate on Mars, *Nature*, **412**, 245–249.
- Lewis, S. R., and P. R. Barker (2005), Atmospheric tides in a Mars general circulation model with data assimilation, *Adv. Space Res.*, **36**, 2162–2168.
- Lewis, S. R., and P. L. Read (1995), An operational data assimilation scheme for the Martian atmosphere, *Adv. Space Res.*, **16**(6), 9–13.
- Lewis, S. R., M. Collins, and P. L. Read (1996), Martian atmospheric data assimilation with a simplified general circulation model: Orbiter and lander networks, *Planet. Space Sci.*, **44**, 1395–1409.
- Lewis, S. R., M. Collins, and P. L. Read (1997), Data assimilation with a Martian atmospheric GCM: An example using thermal data, *Adv. Space Res.*, **19**(8), 1267–1270.
- Magalhães, J. A., J. T. Schofield, and A. Seiff (1999), Results of the Mars Pathfinder atmospheric structure investigation, *J. Geophys. Res.*, **104**(E4), 8943–8956.
- Malin, M. C., and K. S. Edgett (2001), Mars Global Surveyor Mars Orbiter Camera: Interplanetary cruise through primary mission, *J. Geophys. Res.*, **106**(E10), 23,429–23,570.
- Malin, M. C., M. A. Caplinger, and S. D. Davis (2001), Observational evidence for an active surface reservoir of solid carbon dioxide on Mars, *Science*, **294**(5549), 2146–2148.
- McCleese, D. J., et al. (1986), Remote sensing of the atmosphere of Mars using infrared pressure modulation and filter radiometry, *Appl. Opt.*, **25**, 4232–4245.
- McCleese, D. J., R. D. Haskins, J. T. Schofield, R. W. Zurek, C. B. Leovy, D. A. Paige, and F. W. Taylor (1992), Atmosphere and climate studies of Mars using the Mars Observer Pressure Modulated Infrared Radiometer, *J. Geophys. Res.*, **97**, 7735–7757.
- McMahon, S. K. (1996), Overview of the Planetary Data System, *Planet. Space Sci.*, **44**, 3–12.
- Mitrofanov, I., et al. (2002), Maps of subsurface hydrogen from the High Energy Neutron Detector, Mars Odyssey, *Science*, **297**, 78–81.
- Montabone, L., S. R. Lewis, and P. L. Read (2005), Interannual variability of Martian dust storms in assimilation of several years of Mars global surveyor observations, *Adv. Space Res.*, **36**, 2146–2155.
- Montabone, L., S. R. Lewis, P. L. Read, and D. P. Hinson (2006), Validation of Martian meteorological data assimilation for MGS/TES using radio occultation measurements, *Icarus*, **185**, 113–132.
- Paige, D. A., and A. P. Ingersoll (1985), Annual heat balance of Martian polar caps—Viking observations, *Science*, **228**(4704), 1160–1168.
- Paige, D. A., and K. D. Keegan (1994), Thermal and albedo mapping of the polar regions of Mars using Viking Thermal Mapper observations: 2. South polar region, *J. Geophys. Res.*, **99**, 25,993–26,013.
- Paige, D. A., J. E. Bachman, and K. D. Keegan (1994), Thermal and albedo mapping of the polar regions of Mars using Viking Thermal Mapper observations: 1. North polar region, *J. Geophys. Res.*, **99**, 25,959–25,991.
- Palluconi, F. D., and H. H. Kieffer (1979), The climate of the Martian polar cap (abstract), in *Abstracts From the Second International Colloquium Held 15–18 January, 1979 at the California Institute of Technology, Pasadena, CA, NASA Conf. Publ. 2072*, 45–46.
- Rodgers, C. D. (1976), Retrieval of atmospheric temperature and composition from remote measurements of thermal radiation, *Rev. Geophys.*, **14**, 609–624.
- Schofield, J. T., J. R. Barnes, D. Crisp, R. M. Haberle, S. Larsen, J. A. Magalhães, J. R. Murphy, A. Seiff, and G. Wilson (1997), The Mars Pathfinder Atmospheric Structure Investigation/Meteorology (ASI/MET) experiment, *Science*, **278**(5344), 1752–1758.
- Seiff, A., and D. B. Kirk (1977), Structure of the atmosphere of Mars in summer at mid-latitudes, *J. Geophys. Res.*, **82**, 4364–4378.
- Smith, M. D. (2002), The annual cycle of water vapor on Mars as observed by the Thermal Emission Spectrometer, *J. Geophys. Res.*, **107**(E11), 5115, doi:10.1029/2001JE001522.
- Smith, M. D. (2004), Interannual variability in TES atmospheric observations of Mars during 1999–2003, *Icarus*, **167**(1), 148–165.
- Smith, M. D., J. C. Pearl, B. J. Conrath, and P. R. Christensen (2001), One Martian year of atmospheric observations by the Thermal Emission Spectrometer, *Geophys. Res. Lett.*, **28**(22), 4263–4266.
- Taylor, F. W., S. B. Calcutt, P. L. Read, S. R. Lewis, D. J. McCleese, J. T. Schofield, and R. W. Zurek (2006), Atmospheric temperature sounding on Mars, and the Climate Sounder on the 2005 Reconnaissance Orbiter, *Adv. Space Res.*, **38**(4), 713–717.
- Thomas, P. C., and C. Weitz (1989), Sand dune materials and polar layered deposits on Mars, *Icarus*, **81**, 185–215.
- Tillman, J. E. (1988), Mars global atmospheric oscillations: Annually synchronized, transient normal mode oscillations and the triggering of global dust storms, *J. Geophys. Res.*, **93**, 9433–9451.
- Titus, T. N., H. H. Kieffer, and P. R. Christensen (2003), Exposed water ice discovered near the south pole of Mars, *Science*, **299**, 1048–1051.
- Tyler, G. L., G. Balmino, D. P. Hinson, W. L. Sjogren, D. E. Smith, R. A. Simpson, S. W. Asmar, P. Priest, and J. D. Twicken (2001), Radio science observations with Mars Global Surveyor: Orbit insertion through one Mars year in mapping orbit, *J. Geophys. Res.*, **106**(E10), 23,327–23,348.
- Ward, W. R. (1973), Large-scale variations in the obliquity of Mars, *Science*, **181**(4096), 260–262.
- Withers, P., and M. D. Smith (2006), Atmospheric entry profiles from the Mars Exploration Rovers Spirit and Opportunity, *Icarus*, **185**, 133–142.
- Wolff, M. J., and R. T. Clancy (2003), Constraints on the size of Martian aerosols from Thermal Emission Spectrometer observations, *J. Geophys. Res.*, **108**(E9), 5097, doi:10.1029/2003JE002057.
- Zurek, R. W., and L. J. Martin (1993), Interannual variability of planet-encircling dust storms on Mars, *J. Geophys. Res.*, **98**(E2), 3247–3259.
- Zurek, R. W., and S. E. Smrekar (2007), An overview of the Mars Reconnaissance Orbiter (MRO) science mission, *J. Geophys. Res.*, **112**, E05S01, doi:10.1029/2006JE002701.

S. B. Calcutt, P. L. Read, and F. W. Taylor, Department of Physics, University of Oxford, Parks Road, Oxford OX1 3PU, UK.

M. C. Foote, D. M. Kass, D. J. McCleese, J. T. Schofield, and R. W. Zurek, Jet Propulsion Laboratory, California Institute of Technology, 4800 Oak Grove Drive, Pasadena, CA 91109, USA. (Daniel.J.McCleese@jpl.nasa.gov)

C. B. Leovy, Department of Atmospheric Sciences, University of Washington, Box 351640, Seattle, WA 98195, USA.

D. A. Paige, Department of Earth and Space Sciences, University of California, Los Angeles, 595 Charles E. Young Dr. East, 3806 Geology Bldg., P.O. Box 951567, Los Angeles, CA 90095, USA.